Applied Surface Science 688 (2025) 162353

Contents lists available at ScienceDirect

Applied Surface Science

journal homepage: www.elsevier.com/locate/apsusc

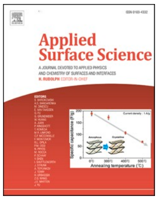

Full Length Article

Enhanced dehydrogenation efficiency in Liquid organic hydrogen Carriers using Sulfur-Doped Pt/TiO_2 Catalysts: A Path to minimizing byproducts[☆]

Yongseok Kim[a], Jeongyeon Heo[a], Purna Chandra Rao[b], Minyoung Yoon[b,*], Kyungsu Na[a,*]

[a] Department of Chemistry, Chonnam National University, Gwangju 61186 Republic of Korea
[b] KNU G-LAMP Research Center, KNU Institute of Basic Sciences, Department of Chemistry, Kyungpook National University, Daegu 41566 Republic of Korea

ARTICLE INFO

Keywords:
Liquid organic hydrogen carrier
Dehydrogenation
Platinum
TiO_2
Byproduct
Sulfur doping

ABSTRACT

The increasing global demand for hydrogen as a sustainable energy carrier has driven the development of advanced hydrogen storage and release technologies. Liquid Organic Hydrogen Carriers (LOHCs), such as methylbenzyl naphthalene (MBN), offer a promising solution due to their high hydrogen storage capacity and favorable dehydrogenation properties. This study investigates the dehydrogenation of perhydro-MBN (H_{16}-MBN) using Pt/TiO_2 catalysts, with an emphasis on enhancing hydrogen yield while minimizing byproduct formation. An exponential increase of byproduct selectivity was observed as the hydrogen yield increased, which should be attributed from the excessive catalytic play of highly active Pt nanoparticles on TiO_2 surface. Through systematic experiments, sulfur-doped Pt/TiO_2 catalysts were found to effectively reduce side reactions and achieve a marked improvement in H_2 yield compared to conventional Pt-based systems, finally escaping from an exponential trend between hydrogen yield and byproduct selectivity. The study reveals that sulfur doping moderates the activity of Pt, thereby suppressing unwanted byproducts and enhancing catalyst stability. These findings underscore the potential of sulfur-doped Pt/TiO_2 catalysts in optimizing LOHC systems, offering a scalable and efficient approach to hydrogen storage and release.

1. Introduction

The global demand for clean and renewable energy has driven extensive research into hydrogen storage and transportation technologies. Among various hydrogen storage methods, Liquid Organic Hydrogen Carriers (LOHCs) have emerged as a promising solution due to their safety, efficiency, and scalability in hydrogen storage and transport [1–9]. A major challenge in developing effective LOHC systems lies in optimizing the dehydrogenation process, which is endothermic, typically requires high temperatures to release hydrogen, and proceeds relatively slower than the hydrogenation process. At the high temperature of dehydrogenation process, it can result in side-reactions that generate undesirable byproducts, thereby reducing overall efficiency [10–12]. Recent studies have highlighted the need for LOHC compounds with lower dehydrogenation enthalpies to minimize energy input, as well as catalysts that selectively promote hydrogen release while suppressing side reactions [5,6,13–16].

Methylbenzyl naphthalene (MBN) has been identified as a promising LOHC compound due to its favorable properties, including a high hydrogen storage capacity of 6.49 wt% and a significantly lower dehydrogenation enthalpy (55.1–55.9 kJ mol^{-1}) compared to other homocyclic LOHCs [17]. However, previous studies have shown that dehydrogenation of perhydro-MBN (i.e., H_{16}-MBN) over Pt-based catalysts, such as Pt/Al_2O_3, Pt/CeO_2, and Pt/TiO_2, leads to the formation of undesirable byproducts, particularly dihydrotetracene (DT) isomers. These byproducts complicate the dehydrogenation process by exceeding the theoretical hydrogen release capacity and forming solid residues, which are difficult to separate from the LOHC system. Furthermore, the sustainable H_2 release/storage using stable LOHCs could not be realized.

The choice of catalyst is crucial for achieving high dehydrogenation efficiency and selectivity in LOHC systems. Pt-based catalysts supported on metal oxides, such as TiO_2, have demonstrated potential in boosting hydrogen yield while minimizing byproduct formation. However, the catalytic performance of Pt/TiO_2 remains slightly inferior to that of Pt/

[☆] This article is part of a special issue entitled: 'MCARE 2024_APSUSC' published in Applied Surface Science.

[*] Corresponding authors.
E-mail addresses: myyoon@knu.ac.kr (M. Yoon), kyungsu_na@chonnam.ac.kr (K. Na).

https://doi.org/10.1016/j.apsusc.2025.162353
Received 31 October 2024; Received in revised form 3 January 2025; Accepted 8 January 2025
Available online 10 January 2025

Al_2O_3 and Pt/CeO_2 catalysts, indicating the need for further optimization. Recently, sulfur doping has been proposed as a strategy to adjust the catalytic activity of Pt by selectively poisoning low-coordinated sites that often exhibit uncontrollable catalytic activity, thereby curbing excessive catalyst activity and mitigating side reactions [18–21]. Auer et al. demonstrated that sulfur selectively modifies Pt/Al_2O_3 catalysts by blocking low-coordinated defect sites, thereby increasing dehydrogenation efficiency and reducing the formation of side-products such as high-boiling components [18]. Similarly, Chen et al. highlighted the effectiveness of sulfur as a selective poison on Pt/TiO_2, where its interaction with the catalyst surface suppresses undesired reactions and enhances hydrogen release efficiency through strong metal-support interactions (SMSI) [19]. Both studies emphasized that the optimal sulfur loading is important to balance the promotion and poisoning effects, which can improve activity, selectivity, and stability of the catalytic systems.

Building upon these findings, this study investigates the dehydrogenation of H_{16}-MBN using sulfur-doped Pt/TiO_2 catalysts to improve hydrogen yield and minimize byproduct formation. We investigate the effects of Pt loading and sulfur doping on the structural and electronic properties of the catalyst, as well as their impact on dehydrogenation performance. Notably, sulfur doping not only significantly reduced the byproduct formation but also enhanced hydrogen yield, demonstrating its dual benefit in optimizing catalytic performance. Through a systematic evaluation of dehydrogenation kinetics at various temperatures, this study aims to provide insights into optimizing catalyst design for efficient hydrogen release in LOHC systems.

2. Experimental section

2.1. Materials preparation

2.1.1. Synthesis of mesoporous TiO_2

Mesoporous TiO_2 was synthesized using a previously reported method [22]. For a typical synthesis of TiO_2, 1.0 g of $HO(CH_2CH_2O)_{20}(CH_2CH(CH_3O)_{70}(CH_2CH_2O)_{20}H$ ($EO_{20}PO_{70}EO_{20}$, triblock copolymer; Pluronic P123, Sigma–Aldrich) was dissolved in 10.0 g of ethanol in a polypropylene bottle. Next, 0.01 mol of titanium precursor ($TiCl_4$ (Daejung)) was added to the obtained solution under vigorous stirring at room temperature for 1 h. The resultant mixture was dispersed in an open Petri dish followed by the gelation at 40 °C in air for 4 d. During gelation, the inorganic precursor was hydrolyzed and polymerized into a metal oxide network that incorporated the P123 triblock copolymer as a mesopore generating agent. Subsequently, the as-prepared bulk samples were calcined at 400 °C for 5 h in air to remove the organic species.

2.1.2. Metal loading

Pt metal nanoparticles were supported on the surface of mesoporous TiO_2 via wet impregnation with desired Pt loadings of 1, 3, and 5 wt%. During impregnation, 1.0 g of mesoporous TiO_2 was suspended in 100.0 mL of deionized water in a round bottomed glass flask. A desired amount of $H_2PtCl_6{\cdot}6H_2O$ (Daejung) was added to this solution, and the resultant mixture was stirred for 1 h at room temperature. The TiO_2 supports impregnated with $H_2PtCl_6{\cdot}6H_2O$ were obtained by evaporating the deionized water using a rotary evaporator at 180 rpm and 60 °C, followed by overnight drying at 100 °C. Subsequently, the Pt metal nanoparticles supported on mesoporous TiO_2 were calcined at 400 °C for 4 h in air. The obtained catalysts were denoted as 1PtT, 3PtT, and 5PtT, where the numbers indicate the Pt loadings (wt%) on the TiO_2 supports. The loading of Pd, Pt-Sn, and Pt-S was carried out in the same manner as the wet impregnation mentioned above, using $PdCl_2$ (Daejung), $SnCl_2$ (Daejung), and $(NH_4)_2SO_4$ (Daejung) as the respective precursors.

2.2. Material characterization

X-ray diffraction (XRD) patterns were acquired using a Rigaku MiniFlex 600 apparatus equipped with Cu Kα radiation ($\lambda = 0.1541$ nm) at 600 W (40 kV, 15 mA). All measurements were conducted under ambient conditions with a step size of 0.005°, a scanning rate of 1° min^{-1}, and a 2θ range spanning from 15 to 80°. The phase compositions were determined using Rietveld refinement techniques through the Rigaku PDXL2 software package. Transmission electron microscopy (TEM) images were obtained using a JEM-2100F instrument (JEOL Ltd.) operating at 200 kV. The elemental composition was determined by energy dispersive spectroscopy (EDS) (X-Max 80 T, Oxford Instruments plc, UK). X-ray photoelectron spectroscopy (XPS) analysis was conducted utilizing a K-ALPHA + instrument (Thermo Fisher Scientific Inc.) equipped with a monochromatic Al Kα source connected to a 128-channel detector. Fresh powder samples were affixed to a stainless-steel sample holder using carbon tape and analyzed under vacuum conditions of 5×10^{-9} mbar. Gaussian − Lorentzian curve fitting was employed for spectral analysis of the Pt 4f, and O 1 s regions after Shirley baseline correction.

2.3. Reaction study

The dehydrogenation of H_{16}-MBN was performed in a laboratory-made automatic reactor system, in which a customized three-neck glass reactor was connected with a reflux condenser, and a mineral oil-containing glass burette was connected with a computer-operated balance [23,24]. H_{16}-MBN was prepared via organic synthesis referring to the literature published elsewhere [17]. The dehydrogenation was monitored in real-time using a computer. For the reaction, Pt metal nanoparticles supported on TiO_2 were reduced under H_2/Ar flows of 60- and 50-mL min^{-1}, respectively, at 350 °C for 2 h with a ramping rate of 3 °C min^{-1}. For a typical reaction process, 4.835 mmol of H_{16}-MBN was added to the catalyst-preloaded reactor. The Pt or Pd metal/reactant (M/R) ratio was 0.27. Before each reaction, the reactor was purged with N_2 to remove air. The reactor was heated to 270 °C, 290 °C, and 310 °C for 25–29 min at a ramping rate of 10 °C min^{-1} using a heating jacket controlled with a proportion–integration–differentiation (PID) temperature controller. The dehydrogenation was performed for 10 h and the H_2 yield was derived by measuring the mass of mineral oil ($d = 0.838$ g mL^{-1} at 25 °C) transferred from the burette to a beaker placed on the balance [23,24]. The volume of H_2 released from the dehydrogenation of H_{16}-MBN was monitored automatically in real-time [23]. GC − mass spectrometry (MS) profiles were recorded on the Agilent 7890A GC with 5975 mass selective detector (MSD) instrument. Rate constants were derived from the linear plots of the H_2 release during the first sharply increasing step at the initial state of dehydrogenation process using a first-order kinetic model using the below equation:

$$k(min^{-1}) = \frac{1}{t_x - t_y} ln(\frac{[H_{16} - MBN]_y}{[H_{16} - MBN]_x})$$

where k is the first-order rate constant, and t_x and t_y are the adjusted time points such that the R-square value exceeds 0.99 for optimal linearity in the kinetic analysis [23].

3. Results and discussion

3.1. Catalysts characterization

The XRD analysis revealed that both mesoporous TiO_2 and Pt/TiO_2 with varying Pt loadings exhibited a typical anatase structure (JCPDS card number 21–1272) (Fig. 1(a)). The minimal structural changes observed across different Pt loadings can be attributed to the SMSI between Pt and TiO_2, which facilitates the uniform dispersion of Pt nanoparticles by stabilizing smaller particles on the TiO_2 surface,

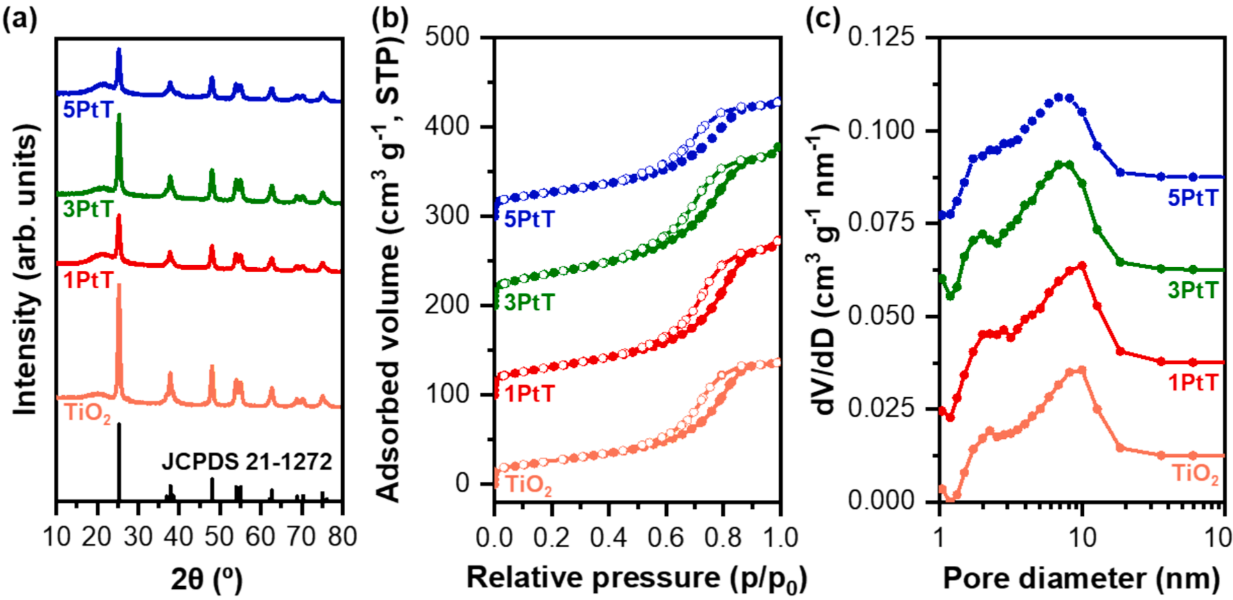

Fig. 1. (a) XRD patterns, (b) N_2 adsorption/desorption isotherms, and (c) their corresponding pore size distributions derived from the desorption branches using the BJH algorithm of mesoporous TiO_2 and Pt/TiO_2 catalysts with various Pt loadings.

thereby making them less visible in the XRD patterns [25–28]. The average particle size of TiO_2, calculated from the TiO_2 (101) plane using the Scherrer equation, was determined to be 10.30 nm. N_2 adsorption/desorption isotherms confirmed a typical type IV hysteresis loop, characteristic of mesoporous structure (Fig. 1(b)). The BET surface area analysis showed comparable values for both TiO_2 and Pt/TiO_2 catalysts, ranging from 96 to 136 m^2 g^{-1}, with an average pore size of approximately 10 nm, as calculated using the BJH method (Fig. 1(c) and Table S1). These findings suggest that the mesoporous structure of TiO_2 results from TiO_2 nanocrystals forming intercrystalline spaces between them. There were no significant changes in intrinsic mesoporous structure and average pore diameter of TiO_2 after supporting Pt metal nanoparticles with various loadings (Fig. 1(c) and Table S1).

TEM analysis of the catalysts revealed that TiO_2 consists of small

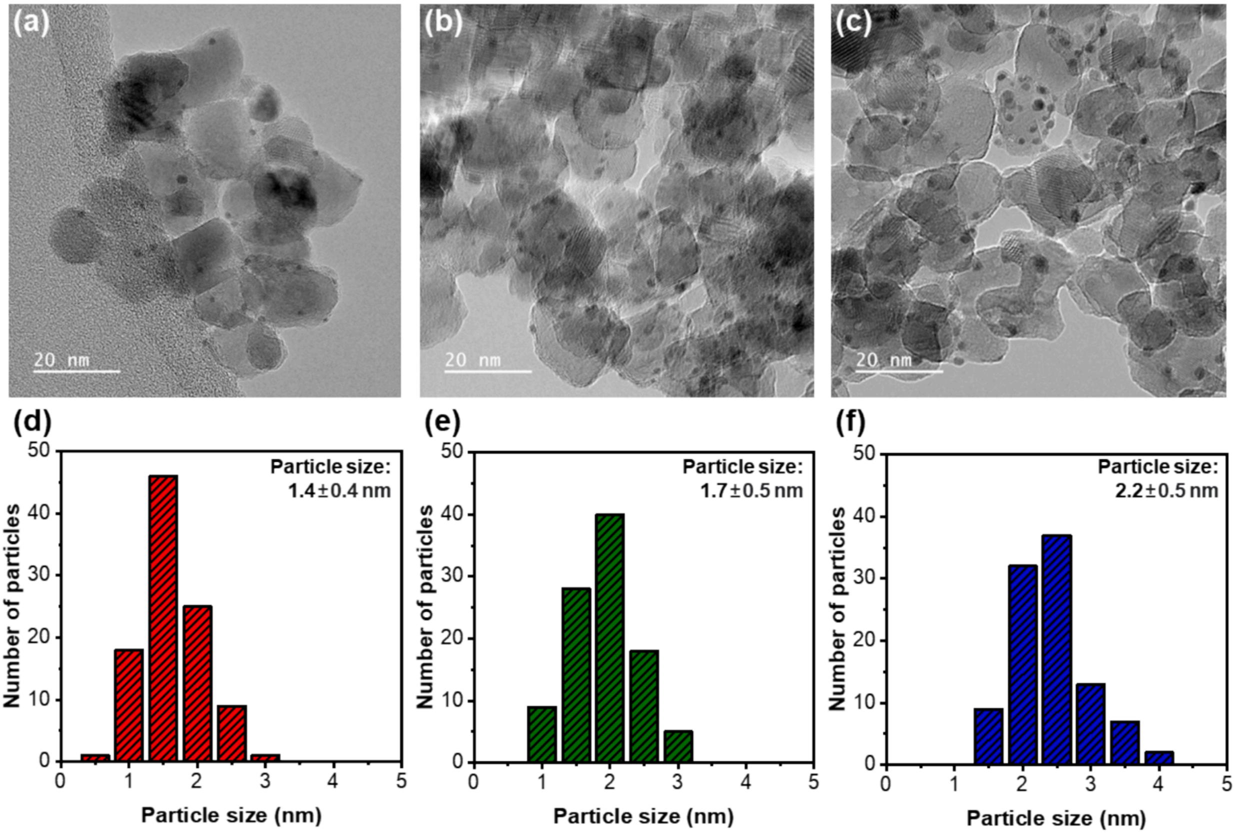

Fig. 2. TEM images of (a) 1PtT, (b) 3PtT, and (c) 5PtT catalysts, and (d–f) their corresponding histograms showing the size distributions of the Pt metal nanoparticles.

crystallites approximately 10–20 nm in size (Fig. 2(a–c)), forming intercrystalline mesopores, consistent with the particle size calculated by the Scherrer equation above. In each Pt-supported TiO_2, Pt metal nanoparticles were dispersed without noticeable ununiform agglomeration. The average particle size systematically increased with 1.4 nm, 1.7 nm, 2.2 nm, as the Pt loading increased with 1, 3, and 5 wt%, respectively (Fig. 2(d–f)). The uniform dispersion of Pt nanoparticles was confirmed by EDS mapping, which showed the Pt nanoparticles were dispersed well throughout the TiO_2 crystals regardless of Pt loadings (Fig. S1–S3). EDS mapping also suggested the Pt loadings of 1.7, 2.7, and 4.1 wt% for 1PtT, 3PtT, and 5PtT, respectively (Table S2–S4).

Electronic properties of reduced PtT catalysts were analyzed using XPS in the Pt 4f region (Fig. S4). The Pt 4f spectra of PtT catalysts were deconvoluted into three peaks, corresponding to Pt^0, $Pt^{\delta+}$, Pt^{2+} and Pt^{4+} at binding energies of approximately 70.6, 71.6. 72.2 and 73.2 eV, respectively (Fig. S4) [29]. By integrating the peak areas and comparing the peak areas, the relative proportions of metallic Pt^0, $Pt^{\delta+}$, Pt^{2+}, and Pt^{4+} were determined (Table S1). As the Pt content supported on TiO_2 increased, Pt exhibited a higher metallic state. This observation is likely due to smaller particle sizes formed at lower Pt loadings and hence SMSI between Pt and TiO_2, which stabilizes Pt in an oxidized state at the interface between Pt and TiO_2 [30,31].

3.2. Dehydrogenation of H_{16}-MBN using Pt/TiO_2 catalysts

In our previous studies, we demonstrated that the newly developed H_{16}-MBN exhibits a faster H_2 release rate and higher H_2 yield compared to perhydro-dibenzyltoluene (H_{16}-DBT), which is attributed to its lower dehydrogenation enthalpy [17]. The dehydrogenation performance of H_{16}-MBN was further evaluated using Pt-supported Al_2O_3, CeO_2, and TiO_2 catalysts (4Pt/Al_2O_3, 2.2Pt/CeO_2 and 1.3Pt/TiO_2 catalysts, containing 4, 2.2 and 1.3 wt% Pt, respectively) (Fig. S5 and Table S5) [17]. It should be noted that due to the significant differences in surface area of metal oxides and hence metal-support interaction with Pt, making a consistent Pt particle size with the same loading in the different metal oxides is difficult. Therefore, Pt nanoparticles were supported to metal oxides with different loadings, resulting in the formation of Pt particle size in the sub-nanometer range (preferably below 3 nm) with a spherical shape [23,32,33]. These catalysts achieved H_2 yields of 94.6 %, 99.3 %, and 85.6 %, respectively. However, GC–MS analysis of the post-reaction solution revealed the presence of unexpected byproducts with a m/z ratio of 230, in addition to the anticipated H_x-MBN species (x = 0, 4, 6, 10, 16) (Fig. 3). If the 100 % of H_{16}-MBN was converted to H_0-MBN with release of desired amount of H_2, only H_0-MBN with m/z ratio of 232 should be detected. However, another product with smaller m/z ratio of 230 were detected in GC–MS chromatogram, suggesting that the H_{16}-MBN was transformed to not only desired MBN but also to undesired compound having smaller molecular weight. In addition, this suggests that the H_2 generated from H_{16}-MBN was resulted not solely from dehydrogenation but also from cyclization reactions, leading to the release of 9 H_2 (from $m/z = 248$ to 230), which exceeds the theoretical limit of 8 H_2 generated from the dehydrogenation of H_{16}-MBN to MBN. The major unexpected dehydrogenated species is suggested by GC–MS as dihydrotetracene (DT, $m/z = 230$) isomers (Fig. 3), which are solid at room temperature, complicating the separation from the LOHC and solid-phase catalyst. Among the evaluated catalysts, TiO_2 showed the lowest production of byproducts, making it as the preferred support material for this study.

The dehydrogenation reaction of H_{16}-MBN were evaluated at various temperatures of 270, 290, and 310 °C using 1PtT, 3PtT, and 5PtT catalysts, with careful attention on the byproduct formation as function of reaction temperatures. At 270 °C, all three catalysts showed similar hydrogen yields and selectivity, around 45 %, with only slight differences in activity (Fig. 4(a)). At 290 °C, the 5PtT catalyst showed a notable increase in H_2 yield, approximately 10 % higher than those of the 1PtT and 3PtT catalysts (Fig. 4(b)). Both 3PtT and 5PtT catalysts demonstrated a rapid increase in H_2 yield during the initial stages of reaction, which was precisely compared with the rate constants (Fig. 4, Table 1 and Fig. S6). Note that the rate constants were derived from the slope of the logarithmic plot of hydrogen concentration versus time using a first-order kinetic model, at an early stage of reaction to obtain the intrinsic catalytic activity excluding the effect of catalyst deactivation. At 310 °C, a similar initial rate constants were observed in all PtT catalysts (Table 1 and Fig. S6), which might be due to the saturation of intrinsic activity of each PtT catalysts (Fig. 4(c)). However, the 1PtT catalyst achieved the highest H_2 yield of 88.6 % at 310 °C. The smaller Pt particle size in 1PtT likely enhances the desorption of intermediates and products, thereby facilitating more efficient adsorption and desorption processes [10,34–36]. However, the larger Pt particle size in other catalysts might adsorb reactant, intermediate, and product species strongly with longer residence time, which would lower the maximum hydrogen yield. The relatively lower performance of the 3PtT catalyst may be attributed to suboptimal particle size and distribution, which is not favorable for optimized adsorption–desorption kinetics despite the higher loadings of Pt compared to 1PtT. This result suggests that desorption of reactant, intermediate and product species play a critical role in maximizing H_2 yield during dehydrogenation of LOHC. Furthermore, it would be highly likely that byproduct formation could be reduced via decreased residence time of desirable dehydrogenated product as adsorbed on the catalyst surface.

Note that, TEM analysis and EDS mapping of 1PtT catalyst showing the highest hydrogen yield at various temperatures confirmed that, after the reaction, Pt nanoparticles in the 1PtT catalyst did not undergo significant agglomeration via thermal sintering (Fig. S7–S8 and Table S6).

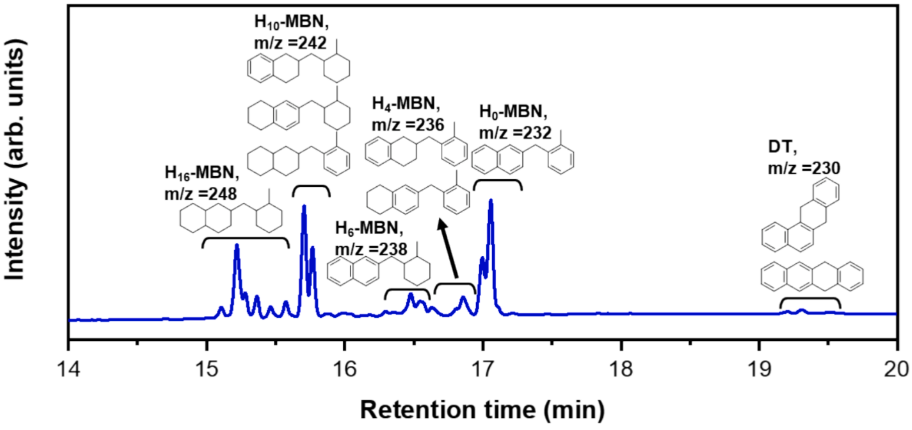

Fig. 3. GC–MS chromatograms showing H_x-MBN (x = 0, 4, 6, 10, 16) and byproducts after dehydrogenation, with their molecular structures with various m/z ratios.

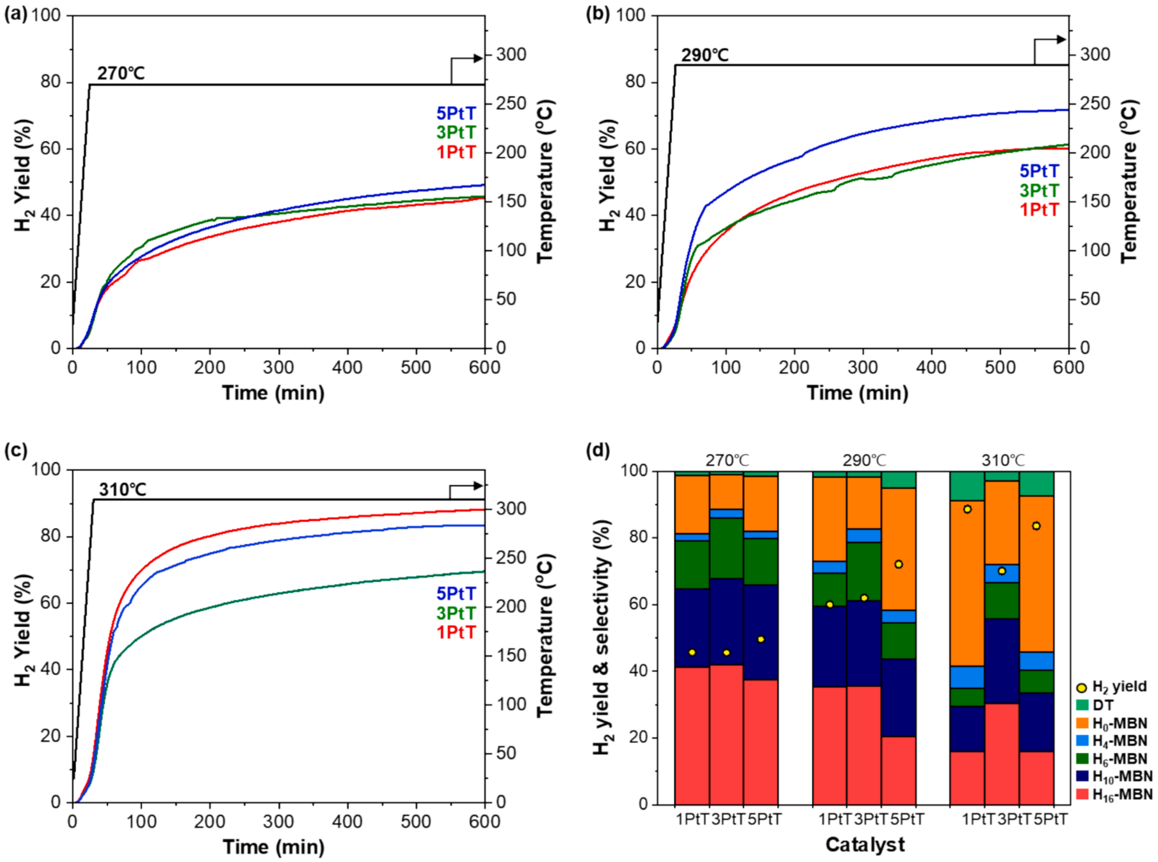

Fig. 4. Time-dependent H_2 release profiles obtained during the dehydrogenation of H_{16}-MBN over various Pt/TiO_2 catalysts at (a) 270, (b) 290, and (c) 310, with (d) their average catalytic performances of H_2 yield, and product selectivity of H_x-MBN ($x = 0, 4, 6, 10, 16$) and byproduct (DT).

Table 1
Catalytic performances of dehydrogenation of H_{16}-MBN using Pt/TiO_2 catalysts.

Catalyst	M/R ratio	MBN (g)	Temp.	Selectivity (%)						H_2 yield (%)	Rate constant (min^{-1})
				H_{16}	H_{10}	H_6	H_4	H_0	DT		
1PtT	0.27	1.3	270	41.3	23.4	14.5	2.1	17.4	1.3	45.7	0.055
			290	35.4	24.2	10.0	3.5	25.2	1.8	60.0	0.056
			310	16.0	13.5	5.5	6.5	49.7	8.8	88.6	0.104
3PtT			270	42.1	25.7	18.2	2.6	10.4	1.0	45.6	0.058
			290	35.6	25.6	17.4	4.1	15.7	1.7	62.0	0.093
			310	30.4	25.3	11.0	5.2	25.1	3.0	70.1	0.097
5PtT			270	37.4	28.5	13.8	2.2	16.6	1.4	49.6	0.065
			290	20.5	23.2	11.0	3.8	36.6	5.0	72.1	0.099
			310	15.9	17.5	7.0	5.3	46.9	7.4	83.6	0.102

Instead, the nanoparticles remained well-dispersed with rather a slight decrease in size. For the 3PtT catalyst, a slight increase in Pt particle size was observed from 1.7 nm to 2.0 nm, while for the 5PtT catalyst, the size increased from 2.2 nm to 2.7 nm (Fig. S9–S12). This observation indicates a strong interaction between Pt nanoparticles and the TiO_2 surface via SMSI effect, even at elevated reaction temperatures up to 310 °C, effectively mitigating sintering and maintaining catalytic performance.

3.3. Breaking an exponential relationship between H_2 yield and byproduct selectivity

To achieve reversible dehydrogenation and hydrogenation of LOHCs for sustainable hydrogen release and storage, it is prerequisite to develop a catalyst with balanced activity and selectivity, maximizing hydrogen yield while minimizing byproduct formation occurring through undesired reaction pathway. Based on our reaction studies above, we plotted catalytic activity, represented by H_2 yield, against byproduct selectivity, represented by DT isomers as the major byproduct, to investigate their relationship (Fig. 5). The maximum H_2 yield obtained from the series of PtT catalysts at three different temperatures of 270 °C, 290 °C, and 310 °C as shown in Table 1, was plotted as a function of byproduct selectivity. The resulting graph shows that byproduct selectivity increases exponentially with increase of H_2 yield. The result clearly suggests that avoiding byproduct formation becomes increasingly challenging as catalytic activity intensifies.

We also prepared two additional catalysts for dehydrogenation of H_{16}-MBN (Fig. 6 and Table S9): TiO_2 supporting 1 wt% of Pd nanoparticles (1PdT), and Sn-doped Pt supported TiO_2 catalyst (1Pt1.8SnT). The first catalyst, Pd on TiO_2, is commonly used for hydrogenation or dehydrogenation reactions, but its catalytic activity differs from Pt-based nanoparticles depending on the target molecules [9,37,38]. When we tested 1PdT at 310 °C, its catalytic activity was significantly lower than that of 1PtT at the same temperature. The byproduct

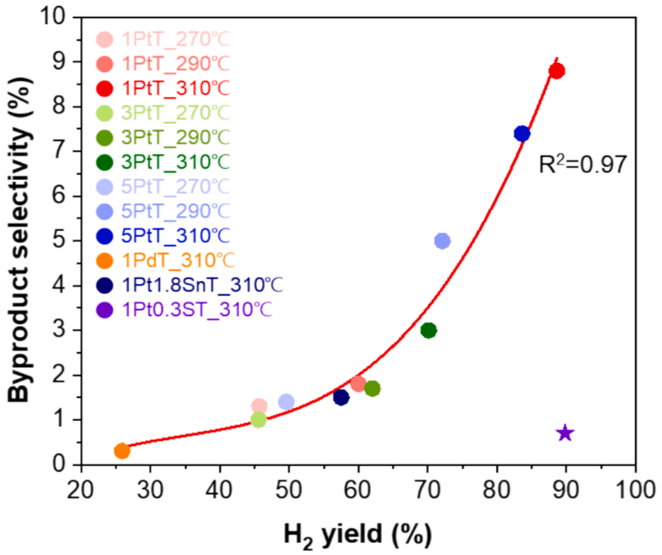

Fig. 5. Relationship between H_2 yield and byproduct selectivity for various Pt/TiO_2 catalysts tested at different temperatures (270, 290, and 310 °C). Catalysts include undoped Pt/TiO_2 with different Pt loadings (1PtT, 3PtT, 5PtT), undoped Pd/TiO_2 (1PdT), Sn-doped Pt (1Pt1.8SnT), and S-doped Pt (1Pt0.3ST) catalysts.

selectivity remained below 0.5 %, but the relationship between H_2 yield and byproduct selectivity still followed an exponential graph, confirming that H_2 yield is still proportional to byproduct selectivity. For the second catalyst, 1.8 wt% of Sn doping into the 1PtT catalyst notably reduced activity compared to the undoped 1PtT (Fig. 6 and Table S9). This reduction in activity is likely due to the dilution of Pt active sites by Sn and the formation of a PtSn alloy [39–43]. Similar to the 1PdT catalyst, the plot of H_2 yield versus byproduct selectivity adhered to the exponential trend, indicating no deviation from the observed relationship.

However, when 0.3 wt% of S (Sulfur) was doped into 1PtT catalyst to create 1Pt0.3ST, the relationship between H_2 yield and byproduct selectivity deviated successfully from the previously observed exponential trend (Fig. 5). The 1Pt0.3ST achieved nearly 90 % of H_2 yield with byproduct selectivity below 1.0 % (Fig. 6 and Table S9). Compared to the 1PtT catalyst, which showed the highest H_2 yield at 310 °C, byproduct selectivity decreased by an order of magnitude, while the catalytic activity remained at approximately 90 % of H_2 yield. It has been widely reported that sulfur can bind readily to low-coordinated sites, such as kinks and edges on the surface of metal nanoparticles, resulting in the selective poisoning of excessively active catalytic sites [18,19,21,44,45]. Accordingly, S doping in 1PtT may possibly poison the active sites responsible for undesired reaction pathways that produce byproducts. Consequently, though the 1Pt0.3ST catalyst exhibited slower dehydrogenation rate than 1PtT (Table S9 and Fig. S13), but it could effectively break free from the exponential relationship between H_2 yield and byproduct selectivity.

Structural characterization of 1Pt0.3ST further corroborates these findings. XRD analysis of the 1Pt0.3ST catalyst revealed a typical anatase structure, with no observable peaks corresponding to the minor amounts of supported Pt and S, even after the reaction (Fig. S14). TEM analysis showed that the average Pt particle size increased only slightly from 1.7 nm before the reaction to 1.8 nm after the reaction, wherein a minimal size change is consistent with the behavior observed in the 1Pt (Fig. S15). EDS analysis confirmed the presence of trace amounts of supported S (Fig. S16–S17 and Table S10–S11). Moreover, XPS analysis of Pt 4f region highlighted key differences between 1PtT and 1Pt0.3ST (Fig. S18). In the 1Pt0.3ST catalyst, the S species were found to adsorb onto the Pt, partially covering the surface and reducing the intensity of the Pt signal. This interaction also altered the electronic environment of Pt atoms, as evidenced by a binding energy shift in the Pt 4f region to higher energy levels [46]. This shift is attributed to charge transfer from Pt to S, further emphasizing the role of S in modulating catalytic behavior.

4. Conclusion

In conclusion, this study highlights the crucial role of catalyst design in optimizing the dehydrogenation processes for LOHC systems, specifically using H_{16}-MBN as the hydrogen carrier. Our findings demonstrate that while increasing Pt content on TiO_2 enhances hydrogen yield, it also leads to an exponential increase in byproduct selectivity, posing a challenge for clean hydrogen production. Through the introduction of sulfur doping, we effectively disrupted this trend, achieving nearly 90 % H_2 yield with significantly reduced byproduct formation. This selective suppression of byproducts via sulfur doping is attributed to the targeted poisoning of highly active sites responsible for undesired reaction pathways. The results emphasize the potential of sulfur-doped Pt/TiO_2 catalysts in balancing activity and selectivity, paving the way for more efficient, scalable, and sustainable LOHC systems that minimize side reactions. Future work will focus on further refining catalyst properties and exploring additional dopants to enhance LOHC performance under varying reaction conditions.

CRediT authorship contribution statement

Yongseok Kim: Writing – review & editing, Writing – original draft, Investigation, Data curation. **Jeongyeon Heo:** Investigation, Data

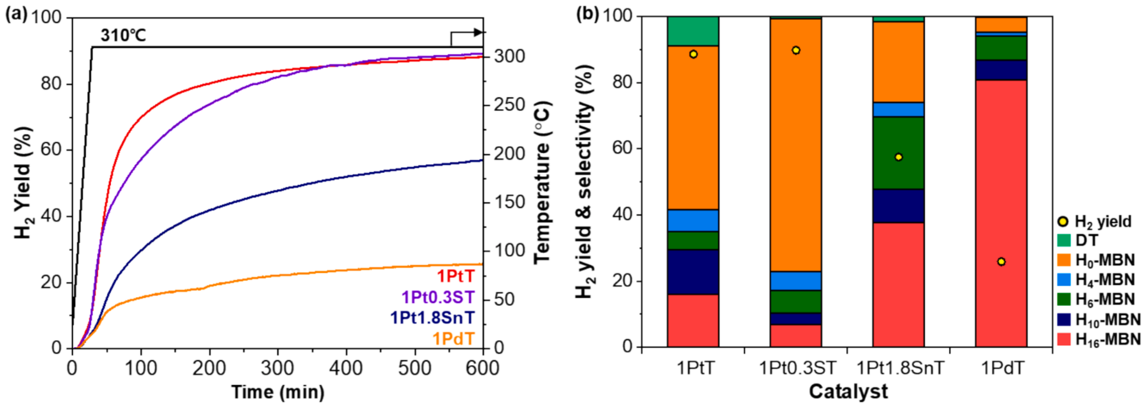

Fig. 6. (a) Time-dependent H_2 release profiles obtained during the dehydrogenation of H_{16}-MBN using 1PtA, 1Pt0.3ST, 1Pt1.8SnT, and 1PdT catalysts, with (b) their average catalytic performances of H_2 yield, and product selectivity of H_x-MBN (x = 0, 4, 6, 10, 16) and byproduct (DT).

curation. **Purna Chandra Rao:** Investigation. **Minyoung Yoon:** Writing – review & editing, Project administration, Funding acquisition. **Kyungsu Na:** Writing – review & editing, Writing – original draft, Project administration, Funding acquisition, Conceptualization.

Declaration of competing interest

The authors declare the following financial interests/personal relationships which may be considered as potential competing interests: [Kyungsu Na reports financial support was provided by National Research Foundation of Korea. Minyoung Yoon reports financial support was provided by National Research Foundation of Korea. If there are other authors, they declare that they have no known competing financial interests or personal relationships that could have appeared to influence the work reported in this paper.].

Acknowledgements

This work was supported by the National Research Foundation of Korea (NRF) grant funded by the Korea government (MSIT) (RS-2024-00349276 and NRF-2019H1D3A1A01102895). This research was supported by "Regional Innovation Strategy (RIS)" through the National Research Foundation of Korea (NRF) funded by the Ministry of Education (MOE) (2021RIS-002). The authors are grateful to the Center of Research Facilities at the Chonnam National University for their assistance in the TEM, and XPS analyses.

Appendix A. Supplementary data

Supplementary data to this article can be found online at https://doi.org/10.1016/j.apsusc.2025.162353.

Data availability

No data was used for the research described in the article.

References

[1] D. Teichmann, W. Arlt, P. Wasserscheid, R. Freymann, A future energy supply based on Liquid Organic Hydrogen Carriers (LOHC), Energy Environ. Sci. 4 (2011) 2767–2773, https://doi.org/10.1039/C1EE01454D.

[2] M. Geißelbrecht, S. Mrusek, K. Müller, P. Preuster, A. Bösmann, P. Wasserscheid, Highly efficient, low-temperature hydrogen release from perhydro-benzyltoluene using reactive distillation, Energy Environ. Sci. 13 (2020) 3119–3128, https://doi.org/10.1039/D0EE01155J.

[3] M. Markiewicz, Y. Zhang, A. Bösmann, N. Brückner, J. Thöming, P. Wasserscheid, S. Stolte, Environmental and health impact assessment of Liquid Organic Hydrogen Carrier (LOHC) systems–challenges and preliminary results, Energy Environ. Sci. 8 (2015) 1035–1045, https://doi.org/10.1039/C4EE03528C.

[4] M. Niermann, S. Drünert, M. Kaltschmitt, K. Bonhoff, Liquid organic hydrogen carriers (LOHCs)–techno-economic analysis of LOHCs in a defined process chain, Energy Environ. Sci. 12 (2019) 290–307, https://doi.org/10.1039/C8EE02700E.

[5] M. Niermann, A. Beckendorff, M. Kaltschmitt, K. Bonhoff, Liquid Organic Hydrogen Carrier (LOHC)–Assessment based on chemical and economic properties, Int. J. Hydrog. Energy 44 (2019) 6631–6654, https://doi.org/10.1016/j.ijhydene.2019.01.199.

[6] P.C. Rao, M. Yoon, Potential liquid-organic hydrogen carrier (LOHC) systems: A review on recent progress, Energies 13 (2020) 6040, https://doi.org/10.3390/en13226040.

[7] J.-Y. Cho, H. Kim, J.-E. Oh, B.Y. Park, Recent advances in homogeneous/heterogeneous catalytic hydrogenation and dehydrogenation for potential liquid organic hydrogen carrier (LOHC) systems, Catalysts 11 (2021) 1497, https://doi.org/10.3390/catal11121497.

[8] P. Preuster, C. Papp, P. Wasserscheid, Liquid Organic Hydrogen Carriers (LOHCs): Toward a Hydrogen-free Hydrogen Economy, Acc. Chem. Res. 50 (2017) 74–85, https://doi.org/10.1021/acs.accounts.6b00474.

[9] Y. Sekine, T. Higo, Recent Trends on the Dehydrogenation Catalysis of Liquid Organic Hydrogen Carrier (LOHC): A Review, Top. Catal. 64 (2021) 470–480, https://doi.org/10.1007/s11244-021-01452-x.

[10] F. Auer, A. Hupfer, A. Bösmann, N. Szesni, P. Wasserscheidpeter, Influence of the nanoparticle size on hydrogen release and side product formation in liquid organic hydrogen carrier systems with supported platinum catalysts, Catal. Sci. Technol. 10 (2020) 6669–6678, https://doi.org/10.1039/D0CY01173H.

[11] T. Solymosi, F. Auer, S. Dürr, P. Preuster, P. Wasserscheid, Catalytically activated stainless steel plates for the dehydrogenation of perhydro dibenzyltoluene, Int. J. Hydrog. Energy 46 (2021) 34797–34806, https://doi.org/10.1016/j.ijhydene.2021.08.040.

[12] J. Bollmann, K. Mitländer, D. Beck, P. Schühle, F. Bauer, L. Zigan, P. Wasserscheid, S. Will, Burner-heated dehydrogenation of a liquid organic hydrogen carrier (LOHC) system, Int. J. Hydrog. Energy 48 (2023) 30039–30056, https://doi.org/10.1016/j.ijhydene.2023.04.062.

[13] V.N. Emel'yanenko, M.A. Varfolomeev, S.P. Verevkin, K. Stark, K. Müller, M. Müller, A. Bösmann, P. Wasserscheid, W. Arlt, Hydrogen Storage: Thermochemical Studies of N-Alkylcarbazoles and Their Derivatives as a Potential Liquid Organic Hydrogen Carriers, J. Phys. Chem. C 119 (2015) 26381–26389. 10.1021/acs.jpcc.5b10392.

[14] S.P. Verevkin, S.P. Safronov, A.A. Samarov, S.V. Vostrikov, Hydrogen storage: Thermodynamic analysis of alkyl-quinolines and alkyl-pyridines as potential liquid organic hydrogen carriers (LOHC), Appl. Sci. 11 (2021) 11758, https://doi.org/10.3390/app112411758.

[15] A.A. Samarov, S.P. Verevkin, Hydrogen storage technologies: Methyl-substituted biphenyls as an auspicious alternative to conventional liquid organic hydrogen carriers (LOHC), J. Chem. Thermodyn. 165 (2022) 106648, https://doi.org/10.1016/j.jct.2021.106648.

[16] M.E. Konnova, S.V. Vostrikov, A.A. Pimerzin, S.P. Verevkin, Thermodynamic analysis of hydrogen storage: Biphenyl as affordable liquid organic hydrogen carrier (LOHC), J. Chem. Thermodyn. 159 (2021) 106455, https://doi.org/10.1016/j.jct.2021.106455.

[17] P.C. Rao, Y. Kim, H. Kim, Y. Son, Y. Choi, K. Na, M. Yoon, Methylbenzyl Naphthalene: Liquid Organic Hydrogen Carrier for Facile Hydrogen Storage and Release, ACS Sustainable Chem. Eng. 11 (2023) 12656–12666, https://doi.org/10.1021/acssuschemeng.3c02689.

[18] F. Auer, D. Blaumeiser, T. Bauer, A. Bösmann, N. Szesni, J. Libuda, P. Wasserscheid, Boosting the activity of hydrogen release from liquid organic hydrogen carrier systems by sulfur-additives to Pt on alumina catalysts, Catal. Sci. Technol. 9 (2019) 3537–3547, https://doi.org/10.1039/C9CY00817A.

[19] X. Chen, C.H. Gierlich, S. Schötz, D. Blaumeiser, T. Bauer, J. Libuda, R. Palkovits, Hydrogen Production Based on Liquid Organic Hydrogen Carriers through Sulfur Doped Platinum Catalysts Supported on TiO_2, ACS Sustainable Chem. Eng. 9 (2021) 6561–6573, https://doi.org/10.1021/acssuschemeng.0c09048.

[20] B. Bong, C. Mebrahtu, D. Jurado, A. Bösmann, P. Wasserscheid, R. Palkovits, Hydrogen Loading and Release Potential of the LOHC System Benzyltoluene/Perhydro Benzyltoluene over S–Pt/TiO_2 Catalyst, ACS Eng. Au 4 (2024) 359–367, https://doi.org/10.1021/acsengineeringau.4c00003.

[21] Y. Jo, T.W. Kim, J. Oh, D. Kim, Y.-W. Suh, Mesoporous sulfur-decorated Pt–Al_2O_3 for dehydrogenation of perhydro benzyltoluenes: Activity-favorable adsorption of reaction species onto electron-deficient Pt atoms, J. Catal. 413 (2022) 127–137, https://doi.org/10.1016/j.jcat.2022.06.025.

[22] P. Yang, D. Zhao, D.I. Margolese, B.F. Chmelka, G.D. Stucky, Generalized syntheses of large-pore mesoporous metal oxides with semicrystalline frameworks, Nature 396 (1998) 152–155, https://doi.org/10.1038/24132.

[23] Y. Kim, Y. Song, Y. Choi, K. Jeong, J.H. Park, K.C. Ko, K. Na, Catalytic consequences of supported Pd catalysts on dehydrogenative H_2 evolution from 2-[(n-Methylcyclohexyl)methyl]piperidine as the liquid organic hydrogen carrier, ACS Sustainable Chem. Eng. 9 (2020) 809–821, https://doi.org/10.1021/acssuschemeng.0c07338.

[24] S. Lim, Y. Song, K. Jeong, J.H. Park, K. Na, Enhanced dehydrogenative H_2 release from N-containing amphicyclic LOHC boosted by Pd-supported nanosheet MFI zeolites having strong acidity and large mesoporosity, ACS Sustainable Chem. Eng. 10 (2022) 3584–3594, https://doi.org/10.1021/acssuschemeng.1c08078.

[25] Y. Lu, H. Deng, T. Pan, L. Wang, C. Zhang, H. He, Interaction between noble metals (Pt, Pd, Rh, Ir, Ag) and defect-enriched TiO_2 and its application in toluene and propene catalytic oxidation, Appl. Surf. Sci. 606 (2022) 154834, https://doi.org/10.1016/j.apsusc.2022.154834.

[26] B. Han, Y. Guo, Y. Huang, W. Xi, J. Xu, J. Luo, H. Qi, Y. Ren, X. Liu, B. Qiao, Strong metal–support interactions between Pt single atoms and TiO_2, Angew. Chem. Int. Ed. 59 (2020) 11824–11829, https://doi.org/10.1002/anie.202003208.

[27] N. Li, Q.-Y. Chen, L.-F. Luo, W.-X. Huang, M.-F. Luo, G.-S. Hu, J.-Q. Lu, Kinetic study and the effect of particle size on low temperature CO oxidation over Pt/TiO_2 catalysts, Appl. Catal. B 142–143 (2013) 523–532, https://doi.org/10.1016/j.apcatb.2013.05.068.

[28] B.K. Singh, S. Lee, K. Na, An overview on metal-related catalysts: metal oxides, nanoporous metals and supported metal nanoparticles on metal organic frameworks and zeolites, Rare Met. 39 (2020) 751–766, https://doi.org/10.1007/s12598-019-01205-6.

[29] R. Mom, L. Frevel, J.-J. Velasco-Vélez, M. Plodinec, A. Knop-Gericke, R. Schlögl, The Oxidation of Platinum under Wet Condition Observed by Electrochemical X-ray Photoelectron Spectroscopy, J. Am. Chem. Soc. 141 (2019) 6537–6544, https://doi.org/10.1021/jacs.8b12284.

[30] X. Gong, Z. Jiang, T. Fang, Enhancing selectivity and reducing cost for dehydrogenation of dodecahydro-N-ethylcarbazole by supporting platinum on titanium dioxide, Int. J. Hydrog. Energy 45 (2020) 6838–6847, https://doi.org/10.1016/j.ijhydene.2019.12.203.

[31] F. Gao, Z. Xu, H. Zhao, Flame spray pyrolysis made Pt/TiO_2 photocatalysts with ultralow platinum loading and high hydrogen production activity, Proc. Combust. Inst. 38 (2021) 6503–6511, https://doi.org/10.1016/j.proci.2020.06.330.

[32] E. Antolini, Structural parameters of supported fuel cell catalysts: The effect of particle size, inter-particle distance and metal loading on catalytic activity and fuel

cell performance, Appl. Catal. B 181 (2016) 298–313, https://doi.org/10.1016/j.apcatb.2015.08.007.

[33] R. Narayana, M.A. El-Sayed, Shape-Dependent Catalytic Activity of Platinum Nanoparticles in Colloidal Solution, Nano Lett. 4 (2004) 1343–1348, https://doi.org/10.1021/nl0495256.

[34] S. Lee, J. Lee, T. Kim, G. Han, J. Lee, K. Lee, J. Bae, Pt/CeO_2 catalyst synthesized by combustion method for dehydrogenation of perhydro-dibenzyltoluene as liquid organic hydrogen carrier: Effect of pore size and metal dispersion, Int. J. Hydrog. Energy 46 (2021) 5520–5529, https://doi.org/10.1016/j.ijhydene.2020.11.038.

[35] Y. Wu, Y. Li, X. Yu, X. Ma, M. Boebinger, J. Weber, Z. Wu, Insights into size effects of Pt/Al_2O_3 catalysts on hydrogen production from methylcyclohexane dehydrogenation, Catal. Sci. Technol. 14 (2024) 1791–1801, https://doi.org/10.1039/D3CY01568H.

[36] J. Oh, Y. Jo, T.W. Kim, H.B. Bathula, S. Yang, J.H. Baik, Y.-W. Suh, Highly efficient and robust Pt ensembles on mesoporous alumina for reversible H_2 charge and release of commercial benzyltoluene molecules, Appl. Catal. B 305 (2022) 121061, https://doi.org/10.1016/j.apcatb.2022.121061.

[37] C.N.M. Ouma, P. Modisha, D. Bessarabov, Insight into the adsorption of a liquid organic hydrogen carrier, perhydro-i-dibenzyltoluene (i= m, o, p), on Pt, Pd and PtPd Planar Surfaces, RSC Adv. 8 (2018) 31895–31904, https://doi.org/10.1039/C8RA05800H.

[38] H. Shuang, H. Chen, F. Wu, J. Li, C. Cheng, H. Li, J. Fu, Catalytic dehydrogenation of hydrogen-rich liquid organic hydrogen carriers by palladium oxide supported on activated carbon, Fuel 275 (2020) 117896, https://doi.org/10.1016/j.fuel.2020.117896.

[39] R. Ryoo, J. Kim, C. Jo, S.W. Han, J.-C. Kim, H. Park, J. Han, H.S. Shin, J.W. Shin, Rare-earth–platinum alloy nanoparticles in mesoporous zeolite for catalysis, Nature 585 (2020) 221–224, https://doi.org/10.1038/s41586-020-2671-4.

[40] L. Deng, T. Arakawa, T. Ohkubo, H. Miura, T. Shishido, S. Hosokawa, K. Teramura, T. Tanaka, Highly active and stable Pt–Sn/SBA-15 catalyst prepared by direct reduction for ethylbenzene dehydrogenation: effects of Sn addition, Ind. Eng. Chem. Res. 56 (2017) 7160–7172, https://doi.org/10.1021/acs.iecr.7b01598.

[41] J. Wu, Z. Peng, A.T. Bell, Effects of composition and metal particle size on ethane dehydrogenation over Pt_xSn_{100-x}/Mg(Al)O ($70\leqslant x\leqslant 100$), J. Catal. 311 (2014) 161–168, https://doi.org/10.1016/j.jcat.2013.11.017.

[42] M.-L. Yang, Y.-A. Zhu, X.-G. Zhou, Z.-J. Sui, D. Chen, First-Principles Calculations of Propane Dehydrogenation over PtSn Catalysts, ACS Catal. 2 (2012) 1247–1258, https://doi.org/10.1021/cs300031d.

[43] A.H. Motagamwala, R. Almallahi, J. Wortman, V.O. Igenegbai, S. Linic, Stable and selective catalysts for propane dehydrogenation operating at thermodynamic limit, Science 373 (2021) 217–222, https://doi.org/10.1126/science.abg7894.

[44] A.J. McCue, J.A. Anderson, Sulfur as a catalyst promoter or selectivity modifier in heterogeneous catalysis, Catal. Sci. Technol. 4 (2014) 272–294, https://doi.org/10.1039/C3CY00754E.

[45] A. Vita, C. Italiano, L. Pino, M. Laganà, V. Recupero, Hydrogen-rich gas production by steam reforming of n-dodecane. Part II: Stability, regenerability and sulfur poisoning of low loading Rh-based catalyst, Appl. Catal. B 218 (2017) 317–326, https://doi.org/10.1016/j.apcatb.2017.06.059.

[46] Q.-Q. Yan, D.-X. Wu, S.-Q. Chu, Z.-Q. Chen, Y. Lin, M.-X. Chen, J. Zhang, X.-J. Wu, H.-W. Liang, Reversing the charge transfer between platinum and sulfur-doped carbon support for electrocatalytic hydrogen evolution, Nat. Commun. 10 (2019) 4977, https://doi.org/10.1038/s41467-019-12851-w.